REVISTA MATÉRIA V.29 N.3
ISSN 1517-7076 articles e20240332, 2024

Enhanced electrochemical performance of Sr doped ZnO for tartrazine detection in sports drink

Jun Dai[1], Yunzhao Liu[1], Erhu Jiang[2]

[1]Hunan University of Foreign Economics, School of Physical Education. Changsha, China.

[2]Ningbo University, School of Sports College. Zhejiang, China.

e-mail: jiangerhu2020@163.com, sunSUN18613735671@hnu.edu.cn, liuyunzhao8223@163.com

ABSTRACT

Tartrazine (Tz) is a widely used synthetic food colorant that has raised health concerns due to its potential adverse effects. Developing sensitive and reliable methods for Tz detection in food products is crucial for ensuring consumer safety. In this study, Sr-doped ZnO nanoparticles with varying doping levels (0–7 mol%) were synthesized by mechanical milling and applied as an electrochemical sensor for detecting Tz in sports drinks. The ZnO-Sr modified carbon paste electrode (CPE), with an optimal Sr doping level of 5 mol%, exhibited the best sensing performance under optimized conditions of pH 7.0 and an accumulation time of 180 s. The sensor demonstrated a linear range from 1 to 1000 µM, a detection limit of 0.3 µM, and a sensitivity of 0.38 µA/µM for Tz identification. This performance surpasses that of many previously reported electrochemical Tz sensors. The ZnO-Sr modified CPE showed good reproducibility (RSD 3.2%), long-term stability (91.2% current retention after one month), and high selectivity against common interferents. The sensor's practical applicability was validated by determining Tz in commercial sports drink samples, with results in good agreement with a standard UV-Vis spectrophotometric method (relative errors < 5%). Recovery tests (97.2–103.5%) further confirmed the accuracy and reliability of the proposed sensor. This work presents a simple, sensitive, and reliable approach for monitoring Tz levels in food products, addressing important food safety and human health concerns.

Keywords: Food colorant sensing; Strontium doping; Electrochemical detection; Carbon paste electrode; Selectivity.

1. INTRODUCTION

Tartrazine (Tz) is a synthetic azo dye commonly used as a colorant in various food products, particularly in soft drinks and sports beverages, due to its bright lemon yellow color, low cost, and good stability [1]. However, the consumption of excessive amounts of Tz has been linked to several health concerns, such as allergic reactions, hyperactivity in children, and potential carcinogenic effects [2]. Therefore, it is crucial to monitor and control the levels of Tz in food and beverages to ensure consumer safety and comply with regulatory standards [3]. Current methods for Tz detection include spectrophotometry, high performance liquid chromatography (HPLC) [4], and capillary electrophoresis [5]. While these techniques are sensitive and reliable, they often require expensive instrumentation, skilled operators, and time-consuming sample preparation procedures. Moreover, they are not suitable for on-site or real-time monitoring of Tz levels in food products. To overcome these limitations, there is a growing interest in developing simple, rapid, and cost-effective methods for Tz detection.

Electrochemical sensors have emerged as a promising alternative to traditional analytical techniques for food quality control and safety assessment [6]. These sensors provide numerous benefits, including excellent sensitivity, strong selectivity, rapid response, ease of portability, and affordability. They can be easily miniaturized and integrated into automated systems for on-site monitoring of food contaminants and additives [7]. Among various electrochemical sensing materials, zinc oxide (ZnO) has attracted significant attention due to its unique properties, such as wide band gap, high electron mobility, and good chemical stability [8]. ZnO is a versatile semiconductor material that has been widely used in photocatalysis, gas sensing, and electrochemical applications [9–11]. Its nanostructured forms, such as nanoparticles, nanorods, and nanoflowers, exhibit enhanced surface area, electrocatalytic activity, and charge transfer efficiency compared to bulk ZnO [12]. However, the performance of ZnO-based electrochemical sensors is often limited by its wide band gap, fast

Corresponding Author: Erhu Jiang Received on 04/06/2024 Accepted on 28/06/2024

DOI: https://doi.org/10.1590/1517-7076-RMAT-2024-0332

electron-hole recombination, and poor electrical conductivity [13]. To address these issues, various strategies have been explored to modify the electronic structure and surface properties of ZnO, such as doping with metal ions, coupling with other semiconductors, and functionalization with conductive polymers or carbon nanomaterials [14].

Incorporating metal ions like Co, Mn, Fe, Cr, Cu, Al, and Sn into ZnO has been shown to enhance its optical, electrical, and catalytic characteristics [15, 16]. Among these dopants, strontium (Sr) is particularly interesting due to its unique electronic configuration and large ionic radius. Sr doping can create defect states within the band gap of ZnO, which can act as electron traps and reduce the recombination of photogenerated charge carriers [17]. Moreover, Sr doping can increase the lattice parameters and surface area of ZnO, which can facilitate the adsorption and diffusion of analyte molecules on the electrode surface [18].

Despite the potential benefits of Sr doping, its application in ZnO-based electrochemical sensors for Tz detection has not been extensively explored. Most of the reported Tz sensors rely on the use of carbon nanomaterials, such as carbon nanotubes, graphene oxide, and carbon quantum dots, as the sensing platform or the electrode modifier [19–26]. While these carbon-based sensors exhibit good sensitivity and selectivity, they often involve complex fabrication processes and may suffer from stability issues in aqueous solutions. In this work, we propose a simple and effective approach to enhance the electrochemical performance of ZnO for Tz detection by doping with Sr ions. Sr-doped ZnO nanoparticles are synthesized using a mechanical milling method followed by heat treatment. The Sr-doped ZnO nanoparticles are then used to modify a carbon paste electrode (CPE) for electrochemical sensing of Tz. The effect of Sr doping percentage on the electrochemical behavior and sensing performance of the modified CPE is systematically investigated using CV and DPV analysis. The optimized sensor is applied for the detection of Tz in real sports drink samples and validated with a standard UV-Vis spectrophotometric method.

The main objectives of this work are: (1) to synthesize and characterize Sr-doped ZnO nanoparticles with enhanced optical and electrochemical properties; (2) to develop a sensitive and selective electrochemical sensor for Tz detection based on Sr-doped ZnO modified CPE; (3) to optimize the sensing parameters and evaluate the analytical performance of the sensor; and (4) to demonstrate the practical applicability of the sensor for Tz detection in real samples. The significance of this work lies in the development of a novel and efficient electrochemical sensing platform for food quality control and safety assessment, which can contribute to the protection of consumer health and the promotion of sustainable food production.

2. MATERIALS AND METHODS

2.1. Synthesis of Sr-doped ZnO nanoparticles

All chemicals used in this study were of analytical grade and used without further purification. $Zn(CH_3COO)_2{\cdot}2H_2O$, $Sr(CH_3COO)_2$, and NaOH were purchased from Aladdin Biochemical Technology Co., Ltd. (Shanghai, China).

Sr-doped ZnO nanoparticles were synthesized by a mechanical milling method followed by heat treatment. In a typical procedure, 5 g of $Zn(CH_3COO)_2{\cdot}2H_2O$ and various amounts of $Sr(CH_3COO)_2$ (0, 1, 3, 5, and 7 mol% relative to Zn) were weighed and mixed in a planetary ball mill with a zirconia milling jar and balls. The milling process was conducted at a rotational speed of 400 rpm for a duration of 4 hours, using a ball-to-powder weight ratio of 10:1. The milled powders were then collected and calcined in a muffle furnace at 500 °C for 2 h with a heating rate of 5 °C/min to obtain Sr-doped ZnO nanoparticles. The samples were labeled as ZnO, ZnO-Sr1, ZnO-Sr3, ZnO-Sr5, and ZnO-Sr7, corresponding to the Sr doping percentage of 0, 1, 3, 5, and 7 mol%, respectively.

2.2. Characterization techniques

The crystal structure and phase purity of the synthesized nanoparticles were characterized by XRD using a Rigaku MiniFlex 600 diffractometer. The lattice parameters, crystallite size, and strain were calculated from the XRD data using the Bragg's law, Scherrer equation, and Williamson-Hall plot, respectively. The morphology and size distribution of the nanoparticles were observed by FE-SEM using a JEOL JSM-7800F microscope operating at an accelerating voltage of 5 kV. The optical properties of the nanoparticles were investigated by UV-Vis DRS and PL spectroscopy.

2.3. Electrode fabrication

CPEs were prepared by mixing graphite powder, Sr-doped ZnO nanoparticles, and paraffin oil in a weight ratio of 70:20:10. The mixture was thoroughly homogenized in a mortar and then packed into a glass tube (inner diameter 3 mm) with a copper wire as the electrical contact. The surface of the CPE was smoothed on a weighing

paper before each measurement. The bare CPE was prepared in the same way without adding Sr-doped ZnO nanoparticles.

2.4. Electrochemical measurements

All electrochemical measurements were performed on a CHI 760A electrochemical workstation (CH Instruments, Shanghai Chenhua). The experiments were carried out in a 0.1 M phosphate buffer solution (PBS, pH 7.0) containing different concentrations of Tz at room temperature. CV was conducted at various scan rates (10–300 mV/s) to investigate the electrochemical behavior of Tz and the effect of Sr doping on the electrode performance. DPV was employed for the quantitative detection of Tz with optimized parameters: amplitude 50 mV, pulse width 0.05 s, sampling width 0.0167 s, and pulse period 0.2 s.

2.5. Tz detection in sports drinks

The practicality of the developed sensor was evaluated by detecting Tz in commercial sports drink samples purchased from a local supermarket. The samples were diluted 10 times with 0.1 M PBS (pH 7.0) before analysis to minimize matrix effects. The content of Tz in the samples was determined by the standard addition method using DPV under optimized conditions. Briefly, aliquots of standard Tz solution were successively added to the diluted sample solution, and the DPV peak currents were recorded after each addition. The Tz concentration in the samples was determined using the linear regression equation derived from the calibration curve, which was created by plotting the peak current versus Tz concentration.

To validate the accuracy of the proposed method, the samples were also analyzed by a reference UV-Vis spectrophotometric method. The samples were diluted appropriately with deionized water, and the absorbance was measured at 427 nm (the maximum absorption wavelength of Tz).

The reproducibility of the sensor was evaluated by fabricating five independent electrodes using the same procedure and measuring their responses to 10 μM Tz. The stability of the sensor was investigated by storing the electrode at 4 °C and measuring its response to 10 μM Tz every day for one week. The effects of common interferents, such as ascorbic acid, citric acid, glucose, and other synthetic food dyes (e.g., sunset yellow and allura red) on the detection of Tz were also examined by DPV under optimized conditions.

3. RESULTS AND DISCUSSION

3.1. Structural and morphological characterization of Sr-doped ZnO

The XRD patterns of pure ZnO and Sr-doped ZnO nanoparticles with different Sr doping percentages (1, 3, 5, and 7 mol%) are shown in Figure 1a. All the samples exhibit sharp and intense diffraction peaks at 2θ values of 31.8°, 34.4°, 36.3°, 47.5°, 56.6°, 62.9°, 66.4°, 67.9°, and 69.1°, which can be indexed to the (100), (002), (101), (102), (110), (103), (200), (112), and (201) planes of ZnO (JCPDS card no. 36–1451) [27]. No characteristic peaks of Sr or other impurities are observed, indicating the successful incorporation of Sr ions into the ZnO lattice without changing its crystal structure. However, a slight shift of the diffraction peaks towards lower angles is observed with increasing Sr doping percentage. This shift indicates an enlargement of the ZnO lattice caused

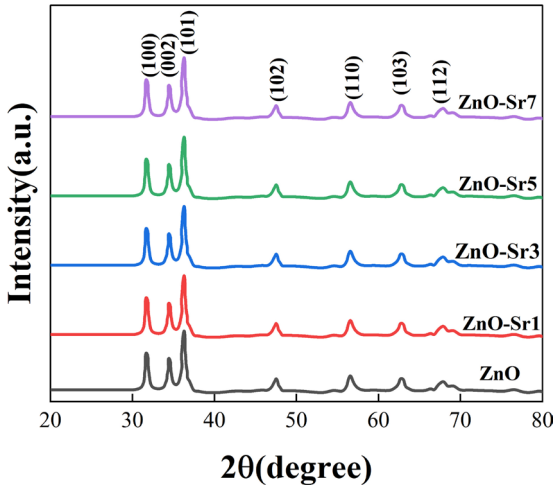

Figure 1: XRD patterns of pure ZnO and Sr-doped ZnO nanoparticles with different Sr doping percentages.

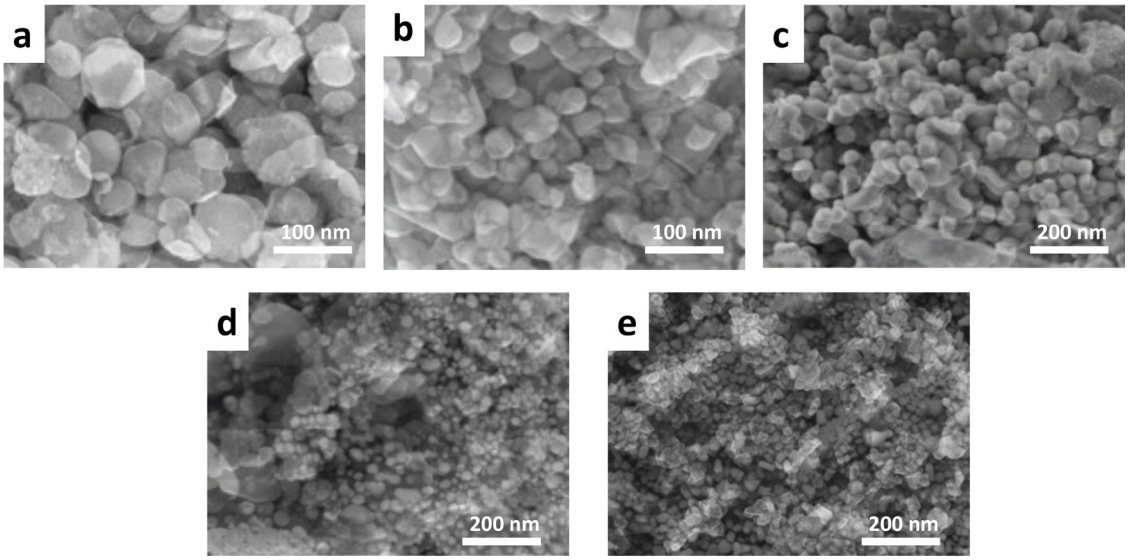

Figure 2: FE-SEM images of (a) pure ZnO, (b) ZnO-Sr1, (c) ZnO-Sr3, (d) ZnO-Sr5, and (e) ZnO-Sr7 nanoparticles.

by the replacement of Zn^{2+} ions (radius 0.74 Å) with the larger Sr^{2+} ions (radius 1.18 Å). The lattice parameters a and c of the samples were calculated from the XRD data and plotted against the Sr doping percentage. Both a and c values increase linearly with increasing Sr content, further confirming the lattice expansion [28]. The crystallite size decreases from 28.5 nm for pure ZnO to 19.2 nm for ZnO-Sr7, indicating that Sr doping suppresses the growth of ZnO nanoparticles. This size reduction can be attributed to the distortion of the ZnO lattice caused by the incorporation of Sr ions, which creates defects and hinders the crystal growth [29].

The morphology and size distribution of pure ZnO and Sr-doped ZnO nanoparticles were characterized by FE-SEM, as shown in Figure 2. Pure ZnO nanoparticles (Figure 2a) display a spherical morphology with an average diameter of 35 nm, which is marginally larger than the crystallite size determined by XRD analysis. This difference suggests that each particle is composed of several crystallites. With increasing Sr doping percentage, the particle size gradually decreases, and the morphology becomes more irregular and aggregated. ZnO-Sr1 (Figure 2b) shows a particle size of 30 nm, while ZnO-Sr3 (Figure 2c) and ZnO-Sr5 (Figure 2d) have particle sizes of 25 nm and 22 nm, respectively. ZnO-Sr7 (Figure 2e) exhibits the smallest particle size of 18 nm, which is consistent with the XRD results. The size reduction and morphology change can be ascribed to the inhibition effect of Sr doping on the growth of ZnO nanoparticles, as well as the increased surface energy and agglomeration tendency of smaller particles [30].

3.2. Optical properties

The optical characteristics of pure ZnO and Sr-doped ZnO nanoparticles were examined using UV-Vis DRS. The UV-Vis DRS spectra of the samples are presented in Figure 3a. All the samples exhibit strong absorption in the UV region due to the band-to-band transition of ZnO. The absorption edge of pure ZnO is located at around 380 nm, corresponding to a band gap energy of 3.26 eV [31]. As the Sr doping percentage increases, the absorption edge progressively shifts to longer wavelengths (red-shift), suggesting a reduction in the band gap [32]. The band gap energies of the samples were estimated from the Tauc plots of $(\alpha h\nu)^2$ versus $h\nu$ (Figure 3b), where α is the absorption coefficient, h is the Planck's constant, and ν is the frequency of light. The band gap values decrease from 3.34 eV for pure ZnO to 3.20, 3.17, 3.16, and 3.18 eV for ZnO-Sr1, ZnO-Sr3, ZnO-Sr5, and ZnO-Sr7, respectively. This band gap narrowing can be attributed to the formation of new energy levels within the band gap of ZnO due to the substitution of Zn^{2+} by Sr^{2+} ions, which have different electronic configurations and orbital energies [33].

PL spectroscopy was employed to study the electron-hole recombination behavior of pure ZnO and Sr-doped ZnO nanoparticles. Figure 4a shows the room-temperature photoluminescence (PL) spectra of the samples excited at 325 nm. The pure ZnO displays a prominent UV emission peak near 380 nm, which is associated with near-band-edge (NBE) emission resulting from the recombination of free excitons [34]. Additionally, a broad visible emission band centered around 550 nm is detected, which is linked to deep-level emission (DLE) caused by intrinsic defects like oxygen vacancies and zinc interstitials [35]. With increasing Sr doping

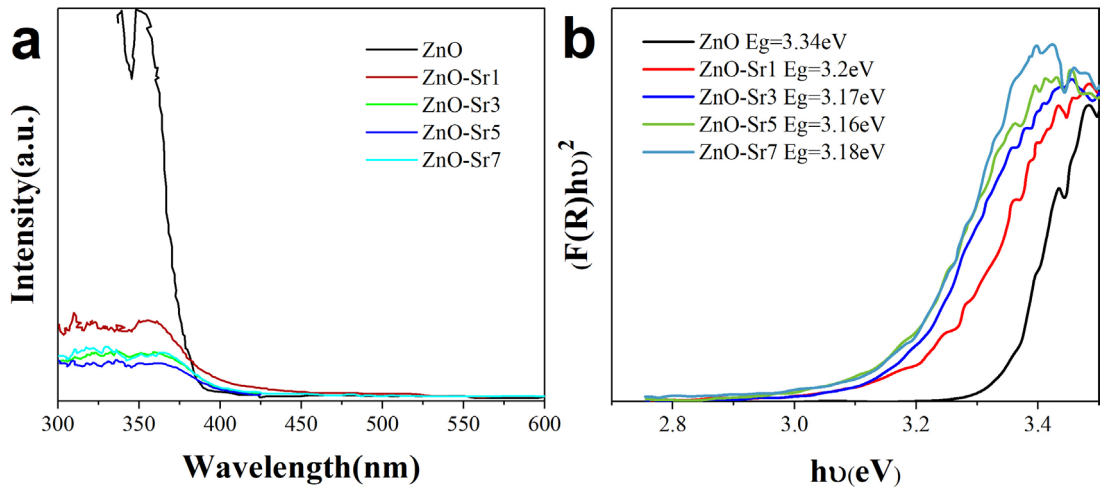

Figure 3: (a) UV-Vis DRS spectra and (b) Tauc plots of pure ZnO nanoparticles and Sr-doped ZnO nanoparticles at varying Sr doping levels.

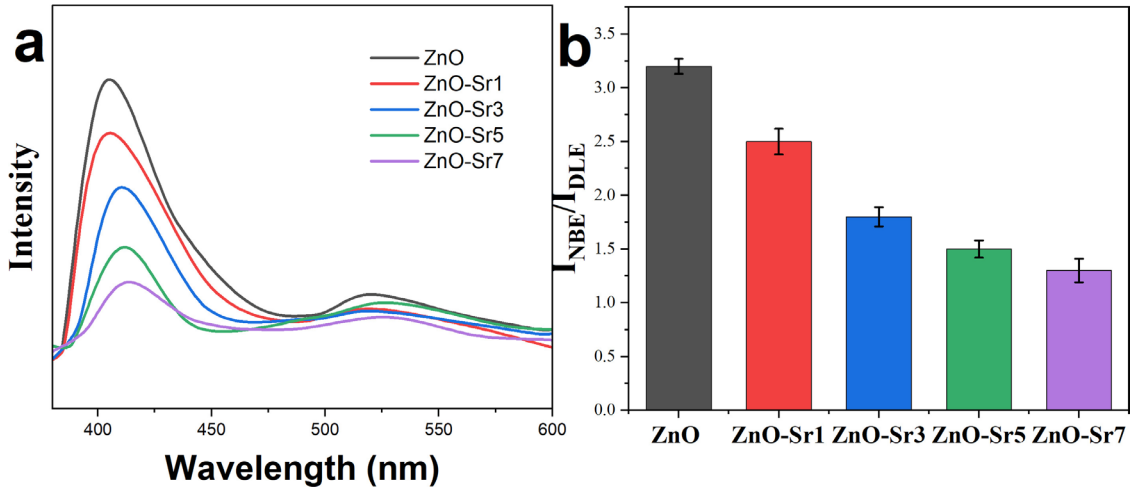

Figure 4: (a) Room-temperature PL spectra and (b) I_{NBE}/I_{DLE}) of pure ZnO and Sr-doped ZnO nanoparticles with different Sr doping percentages.

percentage, the intensity of the NBE emission peak gradually decreases, while the intensity of the DLE band slightly increases. This trend suggests that Sr doping introduces new defect states in the ZnO lattice, which act as electron traps and suppress the radiative recombination of free excitons [36]. The relative intensity ratio of the NBE to DLE emission (I_{NBE}/I_{DLE}) was calculated and plotted against the Sr doping percentage in Figure 4b. The I_{NBE}/I_{DLE} ratio decreases from 3.2 for pure ZnO to 2.5, 1.8, 1.5, and 1.3 for ZnO-Sr1, ZnO-Sr3, ZnO-Sr5, and ZnO-Sr7, respectively, indicating enhanced charge carrier separation and reduced electron-hole recombination with increasing Sr content.

3.3. Electrochemical behavior of Sr-doped ZnO modified CPE

The electrochemical behavior of Tz at the bare CPE and Sr-doped ZnO modified CPEs was examined using cyclic voltammetry (CV) and differential pulse voltammetry (DPV) in 0.1 M PBS (pH 7.0) containing 50 µM Tz. Figure 5a presents the CV curves of various electrodes recorded at a scan rate of 100 mV/s. The bare CPE exhibits a small oxidation peak at around 1.05 V, corresponding to the electrochemical oxidation of Tz. After modification with pure ZnO nanoparticles, the oxidation peak current increases and the peak potential shifts to 0.95 V, indicating the electrocatalytic activity of ZnO towards Tz oxidation. Interestingly, the Sr-doped ZnO modified CPEs show further enhanced oxidation peak currents and reduced peak potentials compared to the pure

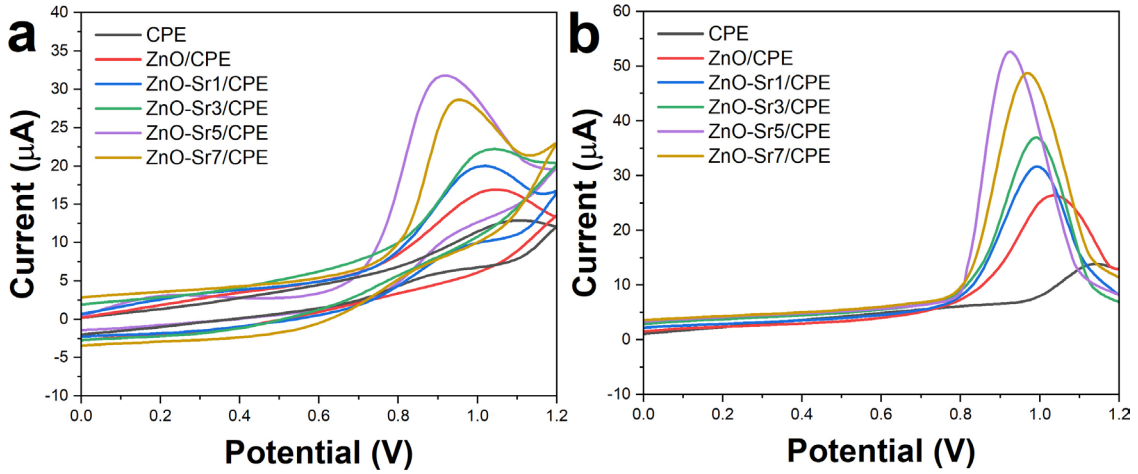

Figure 5: (a) CV and (b) DPV curves of bare CPE, pure ZnO, and Sr-doped ZnO modified CPEs in 0.1 M PBS (pH 7.0) containing 50 μM Tz. Scan rate: 100 mV/s for CV and 10 mV/s for DPV.

ZnO modified CPE. Among them, the ZnO-Sr5 modified CPE achieves the highest peak current and the lowest peak potential of 0.90 V, suggesting its superior electrocatalytic performance for Tz sensing [37–39].

The DPV curves of different electrodes in 50 μM Tz are presented in Figure 5b. Consistent with the CV results, the ZnO-Sr5 modified CPE shows the strongest oxidation peak at 0.8 V with a peak current 3.5 times higher than that of the bare CPE. The enhanced electrochemical response of Sr-doped ZnO modified CPEs can be attributed to the synergistic effect of several factors, including the increased surface area, improved electrical conductivity, reduced electron-hole recombination, and facilitated charge transfer kinetics induced by Sr doping [40–42].

To study the impact of Sr doping levels on the electrochemical sensing performance of ZnO modified CPEs, the oxidation peak currents of 50 μM Tz at various electrodes were measured using DPV and plotted against the Sr doping percentages (Figure 6). The peak current increases with increasing Sr content from 0 to 5 mol%, reaching a maximum value of 54.6 μA at the ZnO-Sr5 modified CPE. This trend can be ascribed to the gradual improvement of the electrical and catalytic properties of ZnO nanoparticles with increasing Sr doping level. However, further increasing the Sr doping percentage to 7 mol% leads to a slight decrease in the peak current to 48.7 μA, which may be due to the excessive defects and grain boundaries introduced by Sr doping that hinder the electron transfer and mass transport processes [43–45]. Therefore, the optimal Sr doping percentage for Tz sensing is determined to be 5 mol%.

The effect of scan rate on the electrochemical behavior of Tz at the ZnO-Sr5 modified CPE was studied by CV to reveal the kinetic characteristics of the electrode reaction. Figure 7 displays the CV curves of 50 μM Tz recorded at different scan rates from 40 to 350 mV/s. With increasing scan rate, the oxidation peak current (Ipa) increases linearly, while the peak potential (Epa) shifts positively. The linear relationship between Ipa and the square root of scan rate ($v^{1/2}$) can be expressed as Ipa (μA) = $2.58v^{1/2}$(mV/s)$^{1/2}$ + 0.47 (R^2 = 0.998). This linear dependence indicates that the oxidation of Tz at the ZnO-Sr5 modified CPE is a diffusion-controlled process [46–48]. The diffusion coefficient of Tz is estimated to be 5.8×10^{-6} cm^2/s, which is higher than those reported for other electrodes, confirming the fast diffusion and efficient mass transport of Tz at the ZnO-Sr5 modified CPE.

To further elucidate the enhanced electrochemical performance of the ZnO-Sr5 modified CPE, we determined the electrochemically active surface area (EASA) of both the bare CPE and the ZnO-Sr5 modified CPE using the Randles-Sevcik equation [49]. The EASA of the ZnO-Sr5 modified CPE (0.186 cm^2) was found to be significantly larger than that of the bare CPE (0.072 cm^2), representing an increase of approximately 158%. This substantial increase in the electroactive surface area contributes to the improved sensing performance of the ZnO-Sr5 modified CPE for Tz detection by providing more active sites for electron transfer and analyte adsorption. We have calculated the surface coverage (Γ) of Tartrazine on the ZnO-Sr5 modified CPE using the following equation:

$$\Gamma = Q/(nFA)$$

where Q is the charge under the oxidation peak (C), n is the number of electrons.

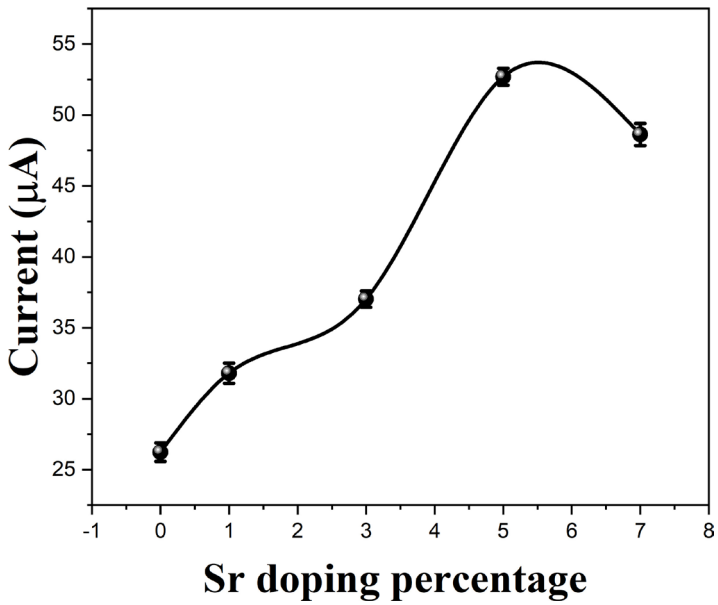

Figure 6: Effect of Sr doping percentage on the DPV oxidation peak current of 50 μM Tz at different Sr-doped ZnO modified CPEs.

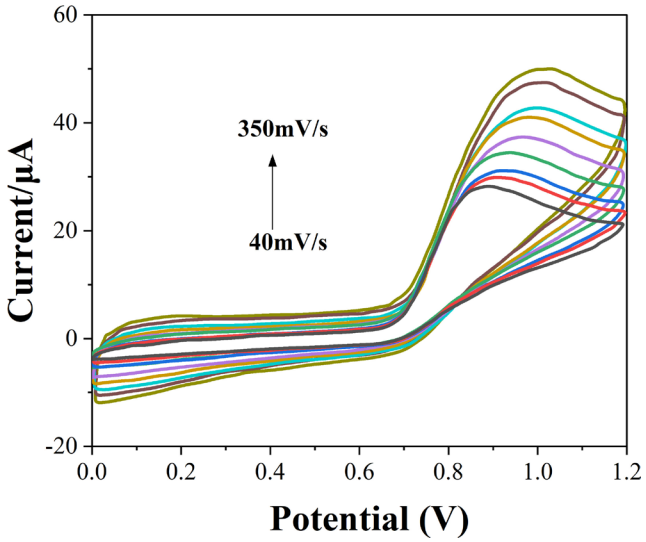

Figure 7: CV curves of 50 μM Tz at the ZnO-Sr5 modified CPE recorded at different scan rates.

We found the surface coverage to be 3.2×10^{-10} mol/cm^2. This value indicates efficient adsorption of Tartrazine on the electrode surface, contributing to the sensor's high sensitivity.

The electrochemical oxidation of Tz at the ZnO-Sr5 modified CPE involves a complex mechanism. Based on our experimental results and previous studies [50, 51], we propose that the oxidation of Tz occurs through an one-electron, one-proton transfer process. The step involves the oxidation of the azo group (-N=N-) in Tz to form a radical cation. This is followed by the loss of a proton, resulting in the formation of an azo radical (Figure 8). The enhanced electrocatalytic activity of the ZnO-Sr5 modified CPE towards Tz oxidation can be attributed to several factors. Firstly, the Sr doping creates oxygen vacancies in the ZnO lattice, which act as active sites for Tz adsorption and electron transfer. Secondly, the increased surface area and improved conductivity of the Sr-doped ZnO nanoparticles facilitate the diffusion and oxidation of Tz molecules. Lastly, the synergistic effect between ZnO and Sr^{2+} ions may promote the formation and stabilization of reaction intermediates, thereby lowering the activation energy for Tz oxidation.

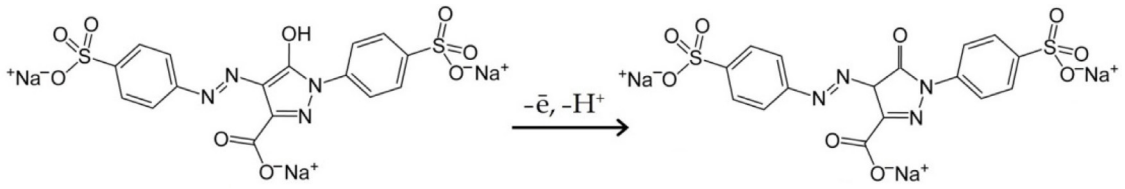

Figure 8: Mechanism of Tz oxidation.

3.4. Optimization of Tz detection parameters

To achieve the best sensing performance, the effects of solution pH, accumulation time, and Sr doping level on the DPV response of Tz at the Sr-doped ZnO modified CPEs were investigated. Figure 9a shows the influence of pH on the oxidation peak current of 50 μM Tz at the ZnO-Sr5 modified CPE in the pH range of 5.0-9.0. The peak current increases with increasing pH from 5.0 to 7.0, reaching a maximum value at pH 7.0, and then decreases with further increasing pH. This trend can be explained by the fact that Tz exists in its anionic form at pH > pKa (7.4), which facilitates its adsorption and oxidation on the positively charged ZnO surface at neutral pH [52].

The effect of accumulation time on the DPV response of 50 μM Tz at the ZnO-Sr5 modified CPE was studied in the range of 0–300 s (Figure 9b). The oxidation peak current increases rapidly with increasing accumulation time up to 180 s, indicating the enhanced adsorption of Tz on the electrode surface. Further prolonging the accumulation time leads to a slight decrease in the peak current, which may be due to the saturation of the electrode surface [53].

Additionally, we optimized the differential pulse voltammetry (DPV) parameters to obtain the best analytical signal for Tz detection. We varied the pulse amplitude (10–100 mV), pulse width (10-100 ms), and step potential (1–10 mV) while measuring the DPV response of 50 μM Tz at the ZnO-Sr5 modified CPE. The optimal parameters were found to be: Pulse amplitude: 50 mV; Pulse width: 50 ms; Step potential: 5 mV. These settings provided the highest peak current and best peak shape for Tz detection. The pulse amplitude of 50 mV offered a good balance between sensitivity and peak resolution. The pulse width of 50 ms allowed sufficient time for faradaic processes while minimizing the contribution of capacitive current. The step potential of 5 mV provided adequate sampling of the voltammogram without excessive noise.

Under the optimized conditions, the DPV responses of Tz at the ZnO-Sr5 modified CPE were recorded in the concentration range of 1–1000 μM (Figure 10a). The oxidation peak current increases linearly with increasing Tz concentration in the range of 0.1–50 μM (Figure 10b). The sensitivity of the ZnO-Sr5 modified CPE is calculated to be 0.38 μA/μM from the slope of the calibration curve. The LOD is estimated to be 0.3 μM, which

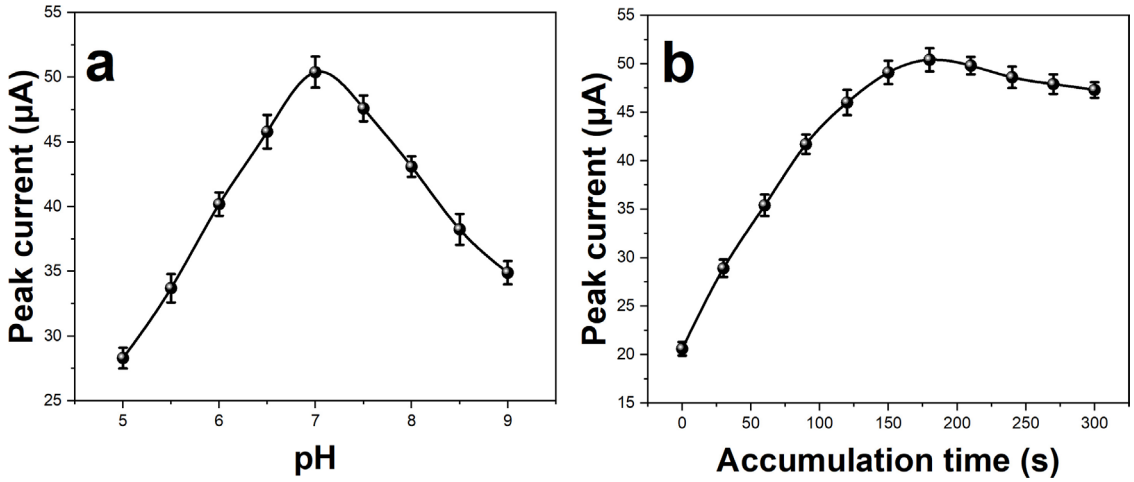

Figure 9: Effects of (a) solution pH and (b) accumulation time on the DPV response of 50 μM Tz at the Sr-doped ZnO modified CPEs.

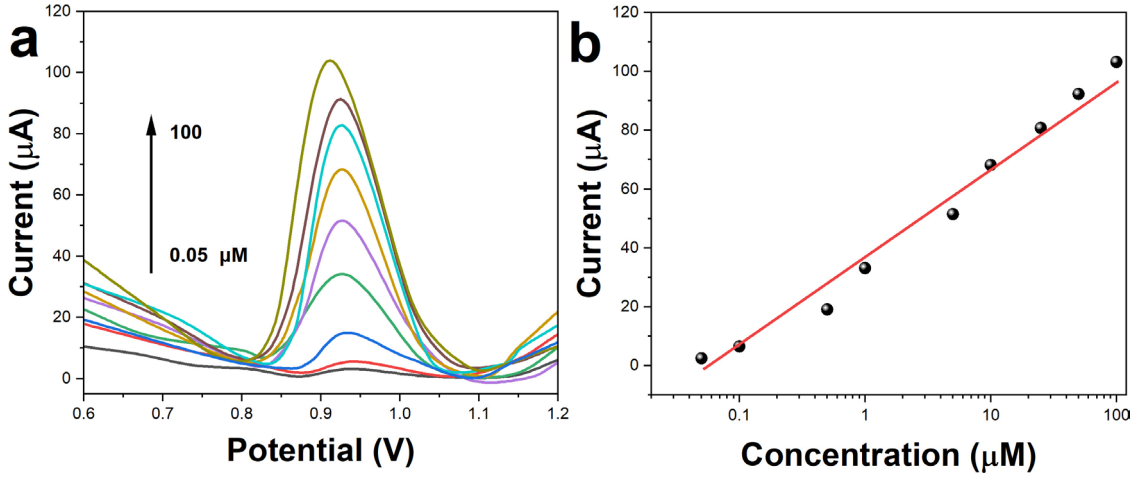

Figure 10: (a) DPV curves of Tz at the ZnO-Sr5 modified CPE in the concentration range of 0.05–100 μM. (b) Linear calibration plot of the oxidation peak current versus Tz concentration.

is lower than the maximum allowable limit of Tz in food products (100 μg/L, 0.2 μM) set by the European Union [54]. The linear range, sensitivity, and LOD of the ZnO-Sr5 modified CPE are superior to those of other electrochemical Tz sensors reported in the literature (Table 1), indicating its great potential for practical applications.

The analytical performance of the ZnO-Sr5 modified CPE for Tz sensing is compared with other recently reported electrochemical Tz sensors based on various nanomaterials (Table 1). The ZnO-Sr5 modified CPE shows a wider linear range, a lower LOD, and a higher sensitivity than most of the other sensors, demonstrating its advantage in terms of detection capability. Moreover, the ZnO-Sr5 modified CPE is facile to fabricate, cost-effective, and environmentally friendly compared to the sensors involving complex modification procedures or expensive materials. Therefore, the Sr-doped ZnO nanoparticles can serve as a promising electrode modifier for the development of high-performance electrochemical sensors for Tz and other food colorants.

3.5. Tz detection in real samples

To assess the real-world applicability of the ZnO-Sr5 modified CPE, it was employed to measure Tz levels in three commercial sports drink samples obtained from a local supermarket. Prior to analysis, the samples were diluted tenfold with the supporting electrolyte (0.1 M PBS, pH 7.0) to reduce matrix effects. The peak currents are proportional to the Tz concentrations in the samples. The Tz contents in the sports drinks were calculated based on the calibration curve and the dilution factor, and the results are listed in Table 2. The detected Tz concentrations range from 12.5 to 32.8 mg/L, which are all below the maximum permissible limit of Tz in soft drinks (100 mg/L) set by the European Union.

To validate the accuracy of the proposed electrochemical method, the Tz concentrations in the sports drink samples were also determined by a standard UV-Vis spectrophotometric method and compared with the DPV results. As shown in Table 2, the Tz concentrations measured by the two methods are in good agreement with relative errors less than 5%, confirming the reliability of the ZnO-Sr5 modified CPE for Tz detection in real samples. Additionally, recovery tests were conducted by adding varying concentrations of Tz standard solutions (5, 10, and 20 mg/L) to the sports drink samples and analyzing these spiked samples using the DPV method. The recoveries range from 97.2% to 103.5% (Table 2), further demonstrating the accuracy and practicality of the proposed sensor.

The reproducibility of the ZnO-Sr5 modified CPE was investigated by comparing the DPV responses of six independently fabricated electrodes towards 50 μM Tz under the optimized conditions. The RSD of the oxidation peak currents was determined to be 3.2%, demonstrating the excellent reproducibility of both the electrode preparation and its sensing performance.The stability of the ZnO-Sr5 modified CPE was evaluated by measuring its DPV response to 50 μM Tz after storage in air at room temperature for different times. As shown in Figure 11c, the peak current retains 95.6% of its initial value after one week and 91.2% after one month, suggesting the excellent long-term stability of the sensor.

The selectivity of the ZnO-Sr5 modified CPE towards Tz was examined by testing its DPV response to 50 μM Tz in the presence of various potential interferents commonly found in sports drinks, such as glucose, fructose, citric acid, ascorbic acid, and other synthetic food dyes (Sunset Yellow and Allura Red).

Table 1: Comparison of the analytical performance of different electrochemical Tz sensors.

ELECTRODE	LINEAR RANGE (µM)	LOD (µM)	REFERENCE
ZnO-Sr5/CPE	1–1000	0.3	This work
MIP-MWNTs-IL@PtNPs/GCE	0.03–5.0 5.0–20.0	0.008	[55]
Gr/PLPA/PGE	2–100	1.54	[56]
CHIT/GO/MWCNTs/AuNPs/GCE	0.02–0.19	0.003	[57]
g-C_3N_4/PGE	0.1–10.0	0.21	[58]
MIP-PmDB/PoPD-GCE	0.005–1.1	0.0035	[59]

Table 2: Determination of Tz in sports drink samples using the ZnO-Sr5 modified CPE and the UV-Vis method, and the recovery test results.

SAMPLE	DETECTED BY DPV (mg/L)	DETECTED BY UV-VIS (mg/L)	RELATIVE ERROR (%)	SPIKED (mg/L)	FOUND (mg/L)	RECOVERY (%)
1	12.5 ± 0.3	12.2 ± 0.2	2.4	5.0	17.3 ± 0.4	98.5
				10.0	22.8 ± 0.5	102.3
				20.0	32.1 ± 0.7	97.2
2	25.6 ± 0.5	26.1 ± 0.4	–1.9	5.0	30.9 ± 0.6	103.5
				10.0	35.3 ± 0.8	97.8
				20.0	45.9 ± 1.1	100.6
3	32.8 ± 0.6	33.4 ± 0.5	–1.8	5.0	37.5 ± 0.7	98.1
				10.0	43.1 ± 0.9	101.2
				20.0	52.4 ± 1.2	98.3

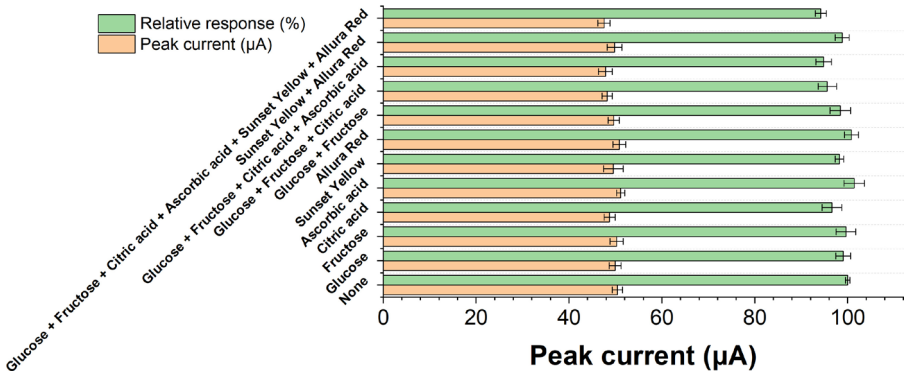

Figure 11: Selectivity test of the ZnO-Sr5 modified CPE for 50 µM Tz detection in the presence of various interferents.

Figure 11 compares the peak currents of Tz before and after the addition of the interferents at concentrations 10 times higher than that of Tz. The changes in the peak currents are all less than ±5%, demonstrating the high selectivity of the sensor for Tz detection. This selectivity can be attributed to the specific interaction and electrocatalytic oxidation of Tz at the Sr-doped ZnO nanoparticles, as well as the low operating potential that avoids the interference from other electroactive substances.

4. CONCLUSION

In conclusion, Sr-doped ZnO nanoparticles with varying Sr doping levels (0–7 mol%) were successfully synthesized by a mechanical milling method and applied as an effective electrode modifier for the electrochemical detection of Tartrazine (Tz) in sports drinks. The ZnO-Sr5 modified CPE, with an optimal Sr doping level of

5 mol%, exhibited the best sensing performance towards Tz under the optimized conditions of pH 7.0 and an accumulation time of 180 s. The ZnO-Sr5 modified CPE showed a wide linear range of 1–1000 μM, a low detection limit of 0.3 μM, and a high sensitivity of 0.38 μA/μM for Tz detection, outperforming most of the previously reported electrochemical Tz sensors. The practical applicability of the ZnO-Sr5 modified CPE was demonstrated by determining Tz in commercial sports drink samples with satisfactory results. The sensor displayed good reproducibility with an RSD of 3.2%, long-term stability with 91.2% current retention after one month, and high selectivity against common interferents. The developed Sr-doped ZnO based electrochemical sensor provides a simple, sensitive, and reliable approach for monitoring Tz levels in food products, which is of great importance for food safety and human health.

5. ACKNOWLEDGEMENTS

This work was supported by Key project of Scientific Research Project of Education Department of Hunan Province “Dynamic Mechanism of Transformation of Sports Scientific and Technological Achievements in Hunan Province under the Background of the New Era” (Project No. 18A485).

6. BIBLIOGRAPHY

[1] PESTANA, S., MOREIRA, M., OLEJ, B., “Safety of ingestion of yellow tartrazine by double-blind placebo controlled challenge in 26 atopic adults”, *Allergologia et Immunopathologia*, v. 38, n. 3, pp. 142–146, May 2010. doi: http://doi.org/10.1016/j.aller.2009.09.009. PubMed PMID: 20106580.

[2] ELHKIM, M.O., HÉRAUD, F., BEMRAH, N., *et al*., “New considerations regarding the risk assessment on Tartrazine: An update toxicological assessment, intolerance reactions and maximum theoretical daily intake in France”, *Regulatory Toxicology and Pharmacology*, v. 47, n. 3, pp. 308–316, Apr. 2007. doi: http://doi.org/10.1016/j.yrtph.2006.11.004. PubMed PMID: 17218045.

[3] KAYA, S.I., CETINKAYA, A., OZKAN, S.A., “Latest advances on the nanomaterials-based electrochemical analysis of azo toxic dyes Sunset Yellow and Tartrazine in food samples”, *Food and Chemical Toxicology*, v. 156, pp. 112524, Oct. 2021. doi: http://doi.org/10.1016/j.fct.2021.112524. PubMed PMID: 34454997.

[4] FIORITO, S., EPIFANO, F., PALUMBO, L., *et al*., “Separation and quantification of Tartrazine (E102) and Brilliant Blue FCF (E133) in green colored foods and beverages”, *Food Research International*, v. 172, pp. 113094, Oct. 2023. doi: http://doi.org/10.1016/j.foodres.2023.113094. PubMed PMID: 37689866.

[5] LIPSKIKH, O.I., KOROTKOVA, E.I., BAREK, J., *et al*., “Simultaneous voltammetric determination of Brilliant Blue FCF and Tartrazine for food quality control”, *Talanta*, v. 218, pp. 121136, Oct. 2020. doi: http://doi.org/10.1016/j.talanta.2020.121136. PubMed PMID: 32797893.

[6] STATE, R.G., VAN STADEN, J., STATE, R.N., *et al*., “Rapid and sensitive electrochemical determination of tartrazine in commercial food samples using IL/AuTiO2/GO composite modified carbon paste electrode”, *Food Chemistry*, v. 385, pp. 132616, Aug. 2022. doi: http://doi.org/10.1016/j.foodchem.2022.132616. PubMed PMID: 35259619.

[7] DE LIMA, L.F., MACIEL, C.C., FERREIRA, A.L., *et al*., “Nickel (II) phthalocyanine-tetrasulfonic-Au nanoparticles nanocomposite film for tartrazine electrochemical sensing”, *Materials Letters*, v. 262, pp. 127186, Mar. 2020. doi: http://doi.org/10.1016/j.matlet.2019.127186.

[8] PAN, Y., ZUO, J., HOU, Z., *et al*., “Preparation of electrochemical sensor based on Zinc oxide nanoparticles for simultaneous determination of AA, DA, and UA”, *Frontiers in Chemistry*, v. 8, pp. 592538, Nov. 2020. doi: http://doi.org/10.3389/fchem.2020.592538. PubMed PMID: 33324612.

[9] PUSHPANJALI, P.A., MANJUNATHA, J.G., AMRUTHA, B.M., *et al*., “Development of carbon nanotube-based polymer-modified electrochemical sensor for the voltammetric study of Curcumin”, *Materials Research Innovations*, v. 25, n. 7, pp. 412–420, Nov. 2021. doi: http://doi.org/10.1080/14328917.2020.1842589.

[10] HAREESHA, N., MANJUNATHA, J.G., “Electro-oxidation of formoterol fumarate on the surface of novel poly(thiazole yellow-G) layered multi-walled carbon nanotube paste electrode”, *Scientific Reports*, v. 11, n. 1, pp. 12797, Jun. 2021. doi: http://doi.org/10.1038/s41598-021-92099-x. PubMed PMID: 34140565.

[11] MANJUNATHA, J.G., DERAMAN, M., BASRI, N.H., “Electrocatalytic detection of dopamine and uric acid at poly (basic blue b) modified carbon nanotube paste electrode”, *Asian Journal of Pharmaceutical and Clinical Research*, v. 8, n. 5, pp. 48–53, 2015.

[12] NUNEZ, F.A., CASTRO, A.C.H., DE OLIVEIRA, V.L., *et al*., "Electrochemical immunosensors based on zinc oxide nanorods for detection of antibodies against SARS-CoV-2 spike protein in convalescent and vaccinated individuals", *ACS Biomaterials Science & Engineering*, v. 9, n. 1, pp. 458–473, Jan. 2023. doi: http://doi.org/10.1021/acsbiomaterials.2c00509. PubMed PMID: 36048716.

[13] NATARAJ, N., CHEN, T.-W., CHEN, S.-M., *et al*., "Synthesis of hexagonal zinc oxide and rod-shaped zinc stannate as an efficient electrocatalyst for electrochemical detection of calcium channel antagonist", *Journal of Molecular Liquids*, v. 385, pp. 122390, Sep. 2023. doi: http://doi.org/10.1016/j.molliq.2023.122390.

[14] CAROFIGLIO, M., BARUI, S., CAUDA, V., *et al*., "Doped zinc oxide nanoparticles: synthesis, characterization and potential use in nanomedicine", *Applied Sciences (Basel, Switzerland)*, v. 10, n. 15, pp. 5194, Jan. 2020. doi: http://doi.org/10.3390/app10155194. PubMed PMID: 33850629.

[15] KUMARI, P., MISRA, K.P., CHATTOPADHYAY, S., *et al*., "A brief review on transition metal ion doped ZnO nanoparticles and its optoelectronic applications", *Materials Today: Proceedings*, v. 43, pp. 3297–3302, Jan. 2021. doi: http://doi.org/10.1016/j.matpr.2021.02.299.

[16] KAREEM, M.A., BELLO, I.T., SHITTU, H.A., *et al*., "Synthesis, characterization, and photocatalytic application of silver doped zinc oxide nanoparticles", *Cleaner Materials*, v. 3, pp. 100041, Mar. 2022. doi: http://doi.org/10.1016/j.clema.2022.100041.

[17] NACIRI, Y., HSINI, A., AJMAL, Z., *et al*., "Influence of Sr-doping on structural, optical and photocatalytic properties of synthesized Ca3(PO4)2", *Journal of Colloid and Interface Science*, v. 572, pp. 269–280, Jul. 2020. doi: http://doi.org/10.1016/j.jcis.2020.03.105. PubMed PMID: 32248078.

[18] MA, J., TAO, Z., KOU, H., *et al*., "Evaluating the effect of Pr-doping on the performance of strontium-doped lanthanum ferrite cathodes for protonic SOFCs", *Ceramics International*, v. 46, n. 3, pp. 4000–4005, Feb. 2020. doi: http://doi.org/10.1016/j.ceramint.2019.10.017.

[19] PUSHPANJALI, P.A., MANJUNATHA, J.G., HAREESHA, N., *et al*., "Voltammetric analysis of antihistamine drug cetirizine and paracetamol at poly(L-Leucine) layered carbon nanotube paste electrode", *Surfaces and Interfaces*, v. 24, pp. 101154, Jun. 2021. doi: http://doi.org/10.1016/j.surfin.2021.101154.

[20] PUSHPANJALI, P.G., MANJUNATHA, J., TIGARI, G., *et al*., "Poly (niacin) based carbon nanotube sensor for the sensitive and selective voltammetric detection of vanillin with caffeine", *Analytical and Bioanalytical Electrochemistry*, v. 12, n. 4, pp. 553–568, 2020.

[21] RARIL, C., MANJUNATHA, J.G., TIGARI, G., "Low-cost voltammetric sensor based on an anionic surfactant modified carbon nanocomposite material for the rapid determination of curcumin in natural food supplement", *Instrumentation Science & Technology*, v. 48, n. 5, pp. 561–582, Sep. 2020. doi: http://doi.org/10.1080/10739149.2020.1756317.

[22] CHARITHRA, M.M., MANJUNATHA, J.G., "Enhanced voltammetric detection of paracetamol by using carbon nanotube modified electrode as an electrochemical sensor", *Journal of Electrochemical Science and Engineering*, v. 10, n. 1, pp. 29–40, 2020. doi: http://doi.org/10.5599/jese.717.

[23] ZOU, Y., GU, H., YANG, J., *et al*., "A high sensitivity strategy of nitrite detection based on CoFe@NC nanocubes modified glassy carbon electrode", *Carbon Letters*, v. 33, n. 7, pp. 2075–2086, Dec. 2023. doi: http://doi.org/10.1007/s42823-023-00558-4.

[24] YI, K., XU, S., CHENG, H., *et al*., "A label-free sensor based on a carbon nanotube-graphene platform for the detection of non-Hodgkin lymphoma genes", *Alexandria Engineering Journal*, v. 84, pp. 93–99, Dec. 2023. doi: http://doi.org/10.1016/j.aej.2023.10.045.

[25] WANG, X., SHI, S., ZHANG, F., *et al*., "Application of a nanotip array-based electrochemical sensing platform for detection of indole derivatives as key indicators of gut microbiota health", *Alexandria Engineering Journal*, v. 85, pp. 294–299, Dec. 2023. doi: http://doi.org/10.1016/j.aej.2023.11.032.

[26] CHEN, L., ZHU, S., WANG, X., "Detection of glioma cells based on electrochemical sensor based on an aptamer method recognition", *International Journal of Electrochemical Science*, v. 17, n. 12, pp. 221258, Dec. 2022. doi: http://doi.org/10.20964/2022.12.59.

[27] YARAHMADI, M., MALEKI-GHALEH, H., MEHR, M.E., *et al*., "Synthesis and characterization of Sr-doped ZnO nanoparticles for photocatalytic applications", *Journal of Alloys and Compounds*, v. 853, pp. 157000, Feb. 2021. doi: http://doi.org/10.1016/j.jallcom.2020.157000.

[28] SATHYA, M., SHOBIKA, P.A., PONNAR, M., *et al*., "Influence of Sr concentration on crystal structure, magnetic properties and supercapacitance performance of ZnO nanoparticles", *Journal of Materials Science Materials in Electronics*, v. 33, n. 9, pp. 6745–6765, Mar. 2022. doi: http://doi.org/10.1007/s10854-022-07852-3.

[29] PRADEEV RAJ, K., SADAIYANDI, K., KENNEDY, A., *et al*., "Structural, optical, photoluminescence and photocatalytic assessment of Sr-doped ZnO nanoparticles", *Materials Chemistry and Physics*, v. 183, pp. 24–36, Nov. 2016. doi: http://doi.org/10.1016/j.matchemphys.2016.07.068.

[30] AKRAM, R., ALMOHAIMEED, Z.M., BASHIR, A., *et al*., "Synthesis and characterization of pristine and strontium-doped zinc oxide nanoparticles for methyl green photo-degradation application", *Nanotechnology*, v. 33, n. 29, pp. 295702, May 2022. doi: http://doi.org/10.1088/1361-6528/ac6760. PubMed PMID: 35504008.

[31] FANG, L., LI, H., MA, X., *et al*., "Optical properties of ultrathin ZnO films fabricated by atomic layer deposition", *Applied Surface Science*, v. 527, pp. 146818, Oct. 2020. doi: http://doi.org/10.1016/j.apsusc.2020.146818.

[32] AZIZAH, N., MUHAMMADY, S., PURBAYANTO, M.A.K., *et al*., "Influence of Al doping on the crystal structure, optical properties, and photodetecting performance of ZnO film", *Progress in Natural Science*, v. 30, n. 1, pp. 28–34, Feb. 2020. doi: http://doi.org/10.1016/j.pnsc.2020.01.006.

[33] GOTO, T., KONDO, Y., CHO, S.H., *et al*., "Comparative study of divalent cation sorption on titania nanotubes using Co^{2+}, Ni^{2+}, Zn^{2+}, and Sr^{2+}", *Chemical Engineering Journal Advances*, v. 12, pp. 100388, Nov. 2022. doi: http://doi.org/10.1016/j.ceja.2022.100388.

[34] HENG, C.L., ZHAO, C.N., ZHANG, L., *et al*., "Effects of Yb doping on the structure and near band-edge emission of ZnO thin films on Si after high temperature annealing", *Journal of Luminescence*, v. 222, pp. 117153, Jun. 2020. doi: http://doi.org/10.1016/j.jlumin.2020.117153.

[35] KUMAWAT, A., MISRA, K.P., CHATTOPADHYAY, S., "Band gap engineering and relationship with luminescence in rare-earth elements doped ZnO: an overview", *Materials Technology*, v. 37, n. 11, pp. 1595–1610, Sep. 2022. doi: http://doi.org/10.1080/10667857.2022.2082351.

[36] WU, S., CHENG, X., LU, Y., *et al*., "Ag localized surface plasma-modulated NBE Emissions from ZnCdO thin films", *Journal of Electronic Materials*, v. 49, n. 8, pp. 4479–4484, Aug. 2020. doi: http://doi.org/10.1007/s11664-020-08057-2.

[37] KHOOBI, A., GHOREISHI, S.M., MASOUM, S., *et al*., "Multivariate curve resolution-alternating least squares assisted by voltammetry for simultaneous determination of betaxolol and atenolol using carbon nanotube paste electrode", *Bioelectrochemistry (Amsterdam, Netherlands)*, v. 94, pp. 100–107, Dec. 2013. doi: http://doi.org/10.1016/j.bioelechem.2013.04.002. PubMed PMID: 23632433.

[38] GHOREISHI, S.M., BEHPOUR, M., KHOOBI, A., *et al*., "Determination of trace amounts of sulfamethizole using a multi-walled carbon nanotube modified electrode: application of experimental design in voltammetric studies", *Analytical Letters*, v. 46, n. 2, pp. 323–339, Jan. 2013. doi: http://doi.org/10.1080/00032719.2012.718831.

[39] GHOREISHI, S.M., BEHPOUR, M., KHOOBI, A., "Central composite rotatable design in the development of a new method for optimization, voltammetric determination and electrochemical behavior of betaxolol in the presence of acetaminophen based on a gold nanoparticle modified electrode", *Analytical Methods*, v. 4, n. 8, pp. 2475–2485, Jul. 2012. doi: http://doi.org/10.1039/c2ay25268f.

[40] MOLLAEI, M., GHOREISHI, S.M., KHOOBI, A., "Electrochemical investigation of a novel surfactant for sensitive detection of folic acid in pharmaceutical and biological samples by multivariate optimization", *Measurement*, v. 145, pp. 300–310, Oct. 2019. doi: http://doi.org/10.1016/j.measurement.2019.05.064.

[41] SUBAK, H., TALAY PINAR, P., "Electrochemical behavior of janus kinase inhibitor ruxolitinib at a taurine-electropolymerized carbon paste electrode: insights into sensing mechanisms", *ACS Applied Bio Materials*, v. 7, n. 5, pp. 3179–3189, May 2024. doi: http://doi.org/10.1021/acsabm.4c00186. PubMed PMID: 38581305.

[42] VALIAN, M., KHOOBI, A., SALAVATI-NIASARI, M., "Synthesis, characterization and electrochemical sensors application of Tb2Ti2O7 nanoparticle modified carbon paste electrode for the sensing of mefenamic acid drug in biological samples and pharmaceutical industry wastewater", *Talanta*, v. 247, pp. 123593, Sep. 2022. doi: http://doi.org/10.1016/j.talanta.2022.123593. PubMed PMID: 35636361.

[43] KHOOBI, A., SOLTANI, N., AGHAEI, M., "Computational design and multivariate statistical analysis for electrochemical sensing platform of iron oxide nanoparticles in sensitive detection of anti-inflammatory drug diclofenac in biological fluids", *Journal of Alloys and Compounds*, v. 831, pp. 154715, Aug. 2020. doi: http://doi.org/10.1016/j.jallcom.2020.154715.

[44] TAJIK, S., TAHER, M.A., BEITOLLAHI, H., "The first electrochemical sensor for determination of mangiferin based on an ionic liquid-graphene nanosheets paste electrode", *Ionics*, v. 20, n. 8, pp. 1155–1161, Aug. 2014. doi: http://doi.org/10.1007/s11581-013-1063-2.

[45] BEITOLLAHI, H., TAJIK, S., PARVAN, H., *et al*., "Nanostructured based electrochemical sensor for voltammetric determination of ascorbic acid in pharmaceutical and biological samples", *Analytical and Bioanalytical Electrochemistry*, v. 6, n. 1, pp. 54–66, 2014.

[46] MAHMOUDI MOGHADDAM, H., BEITOLLAHI, H., TAJIK, S., *et al*., "Fabrication of novel TiO2 nanoparticles/Mn(III) salen doped carbon paste electrode: application as electrochemical sensor for the determination of hydrazine in the presence of phenol", *Environmental Monitoring and Assessment*, v. 187, n. 7, pp. 407, Jun. 2015. doi: http://doi.org/10.1007/s10661-015-4629-9. PubMed PMID: 26045039.

[47] TAJIK, S., BEITOLLAHI, H., SHAHSAVARI, S., *et al*., "Simultaneous and selective electrochemical sensing of methotrexate and folic acid in biological fluids and pharmaceutical samples using Fe_3O_4/ppy/Pd nanocomposite modified screen printed graphite electrode", *Chemosphere*, v. 291, n. Pt 3, pp. 132736, Mar. 2022. doi: http://doi.org/10.1016/j.chemosphere.2021.132736. PubMed PMID: 34728224.

[48] VENKATRAMANAN, S., CHUNG, S.Y., RAMKUMAR, T., *et al*., "Environmental monitoring and assessment of heavy metals in surface sediments at Coleroon River Estuary in Tamil Nadu, India", *Environmental Monitoring and Assessment*, v. 187, n. 8, pp. 505, Jul. 2015. doi: http://doi.org/10.1007/s10661-015-4709-x. PubMed PMID: 26178040.

[49] TAJIK, S., DOURANDISH, Z., GARKANI NEJAD, F., *et al*., "Transition metal dichalcogenides: Synthesis and use in the development of electrochemical sensors and biosensors", *Biosensors & Bioelectronics*, v. 216, pp. 114674, Nov. 2022. doi: http://doi.org/10.1016/j.bios.2022.114674. PubMed PMID: 36095980.

[50] BONYADI, S., GHANBARI, K., "Application of molecularly imprinted polymer and ZnO nanoparticles as a novel electrochemical sensor for tartrazine determination", *Microchemical Journal*, v. 187, pp. 108398, Apr. 2023. doi: http://doi.org/10.1016/j.microc.2023.108398.

[51] STOZHKO, N.Y., KHAMZINA, E.I., BUKHARINOVA, M.A., *et al*., "An electrochemical sensor based on carbon paper modified with graphite powder for sensitive determination of sunset yellow and tartrazine in drinks", *Sensors (Basel)*, v. 22, n. 11, pp. 4092, Jan. 2022. doi: http://doi.org/10.3390/s22114092. PubMed PMID: 35684711.

[52] WU, S., YIN, Z.-Z., CHEN, X., *et al*., "Electropolymerized melamine for simultaneous determination of nitrite and tartrazine", *Food Chemistry*, v. 333, pp. 127532, Dec. 2020. doi: http://doi.org/10.1016/j.foodchem.2020.127532. PubMed PMID: 32668396.

[53] HE, Q., LIU, J., LIU, X., *et al*., "Sensitive and selective detection of tartrazine based on TiO2-electrochemically reduced graphene oxide composite-modified electrodes", *Sensors (Basel)*, v. 18, n. 6, pp. 1911, Jun. 2018. doi: http://doi.org/10.3390/s18061911. PubMed PMID: 29895779.

[54] AHMAD, I., MURTAZA, S., AHMED, S., "Electrochemical and photovoltaic study of sunset yellow and tartrazine dyes", *Monatshefte für Chemie*, v. 146, n. 10, pp. 1631–1640, 2015. doi: http://doi.org/10.1007/s00706-015-1425-8.

[55] ZHAO, L., ZENG, B., ZHAO, F., "Electrochemical determination of tartrazine using a molecularly imprinted polymer – multiwalled carbon nanotubes – ionic liquid supported Pt nanoparticles composite film coated electrode", *Electrochimica Acta*, v. 146, pp. 611–617, Nov. 2014. doi: http://doi.org/10.1016/j.electacta.2014.08.108.

[56] TAHTAISLEYEN, S., GORDUK, O., SAHIN, Y., "Electrochemical determination of tartrazine using a graphene/poly(l-phenylalanine) modified pencil graphite electrode", *Analytical Letters*, v. 53, n. 11, pp. 1683-1703, Jul. 2020. doi: http://doi.org/10.1080/00032719.2020.1716242.

[57] ROVINA, K., SIDDIQUEE, S., MD SHAARANI, S., "An electrochemical sensor for the determination of tartrazine based on CHIT/GO/MWCNTs/AuNPs composite film modified glassy carbon electrode", *Drug and Chemical Toxicology*, v. 44, n. 5, pp. 447–457, Sep. 2021. doi: http://doi.org/10.1080/01480545.2019.1601210. PubMed PMID: 31020858.

[58] KARIMI, M.A., AGHAEI, V.H., NEZHADALI, A., *et al*., "Graphitic carbon nitride as a new sensitive material for electrochemical determination of trace amounts of tartrazine in food samples", *Food Analytical Methods*, v. 11, n. 10, pp. 2907–2915, Oct. 2018. doi: http://doi.org/10.1007/s12161-018-1264-4.

[59] ZHAO, X., LIU, Y., ZUO, J., *et al*., "Rapid and sensitive determination of tartrazine using a molecularly imprinted copolymer modified carbon electrode (MIP-PmDB/PoPD-GCE)", *Journal of Electroanalytical Chemistry (Lausanne, Switzerland)*, v. 785, pp. 90–95, Jan. 2017. doi: http://doi.org/10.1016/j.jelechem.2016.12.015.